

# A possible dynamically Cold Classical contact binary: (126719) 2002 CC<sub>249</sub>.

Audrey Thirouin<sup>1</sup>

*Lowell Observatory, 1400 W Mars Hill Rd, Flagstaff, Arizona, 86001, USA.*

thirouin@lowell.edu

and

Scott S. Sheppard<sup>2</sup>

*Department of Terrestrial Magnetism (DTM), Carnegie Institution for Science, 5241 Broad Branch Rd. NW, Washington, District of Columbia, 20015, USA.*

ssheppard@carnegiescience.edu

## ABSTRACT

Images of the Kuiper belt object (126719) 2002 CC<sub>249</sub> obtained in 2016 and 2017 using the 6.5m Magellan-Baade Telescope and the 4.3m Discovery Channel Telescope are presented. A lightcurve with a periodicity of  $11.87 \pm 0.01$  h and a peak-to-peak amplitude of  $0.79 \pm 0.04$  mag is reported. This high amplitude double-peaked lightcurve can be due to a single elongated body, but it is best explained by a contact binary system from its U-/V-shaped lightcurve. We present a simple full-width-at-half-maximum (FWHM) test that can be used to determine if an object is likely a contact binary or an elongated object based on its lightcurve. Considering that 2002 CC<sub>249</sub> is in hydrostatic equilibrium, a system with a mass ratio  $q_{min}=0.6$ , and a density  $\rho_{min}=1$  g cm<sup>3</sup>, or less plausible a system with  $q_{max}=1$ , and  $\rho_{max}=5$  g cm<sup>3</sup> can interpret the lightcurve. Assuming a single Jacobi ellipsoid in hydrostatic equilibrium, and an equatorial view, we estimate  $\rho \geq 0.34$  g cm<sup>-3</sup>, and  $a/b=2.07$ . Finally, we report a new color study showing that 2002 CC<sub>249</sub> displays an ultra red surface characteristic of a dynamically Cold Classical trans-Neptunian object.

*Subject headings:* Kuiper Belt Objects: (126719) 2002 CC<sub>249</sub>, Techniques: photometric

## 1. Introduction

The trans-Neptunian (or Kuiper) belt is structured in four dynamical groups: i) *classical trans-Neptunian Objects (TNOs)* are between 40 and 48 AU, and are not significantly perturbed by Neptune or captured in a mean motion resonance with Neptune. Their orbits have low inclinations and are almost circular (typically with eccentricity  $< 0.3$ ), ii) *resonant TNOs* are trapped in a resonance with Neptune and thus have had significant interactions with Neptune in the past, iii) *scattered disk TNOs* have large inclinations and eccentricities, with perihelia near Neptune's orbit, suggest-

ing they were scattered by Neptune in the past and iv) *extreme or detached TNOs* with highly eccentric orbits present perihelion distances ( $q > 40$  AU) beyond the Neptune gravitational influence.

Based on orbital inclination, size and color studies of objects in the classical belt, at least two sub-populations have been identified (Peixinho et al. 2008; Brown 2001; Levison & Stern 2001): i) the Hot classical TNOs are dynamically excited, have high orbital inclination and eccentricity and were likely scattered by the giant planets and captured into the trans-Neptunian population, ii) the Cold Classical TNOs at low inclinations appear more primordial, are small, and are red (Batygin

et al. 2011; Benecchi et al. 2009; Noll et al. 2008a).

Among the Cold Classical population, the separated binary fraction is high, about 20-25% but in the other dynamical groups the percentage is only 5-10% (Noll et al. 2008a). Most of the binary Cold Classicals are wide equal-sized binaries with primary and secondary having comparable sizes. In the trans-Neptunian belt, the contact binary population remains elusive. The first and unique confirmed contact binary is 2001 QG<sub>298</sub> (an object in the 3:2 mean motion resonance with Neptune) whereas 2003 SQ<sub>317</sub> (a Haumea family member, dynamically Hot Classical), and 2004 TT<sub>357</sub> (an object in the 5:2 mean motion resonance with Neptune) are likely contact binaries (Sheppard & Jewitt 2004; Lacerda et al. 2014; Thirouin et al. 2017). Surprisingly, none of these objects are in the dynamically Cold Classical sub-population, where the highest fraction of wide binaries is seen.

2002 CC<sub>249</sub> is a dynamical Cold Classical TNO with a semi-major axis<sup>1</sup> of 47.44 AU, an inclination of 0.84°, and an eccentricity of 0.20 (Gladman et al. 2008). Based on *Hubble Space Telescope* images, no companion orbiting 2002 CC<sub>249</sub> was detected (Noll et al. 2008b).

Following, we present the lightcurve of 2002 CC<sub>249</sub> based on observations carried out since 2016. The lightcurve has a large variability caused by an egg-shaped object or more likely by a binary system in close configuration. We also report new color estimates for this object. Next, we describe our observations, and the data reduction techniques. Sections 3 and 4 present and analyze the lightcurve and the colors of 2002 CC<sub>249</sub>. Finally, we summarize our results in the latest section of this paper.

## 2. Observations and analysis

We present in-situ observations carried out with the Discovery Channel Telescope (DCT) and the 6.5 m Magellan Telescope (Baade unit) in 2016 and in 2017.

The DCT is located in Arizona (Happy Jack, United States of America). Our observations were obtained with the Large Monolithic Imager (LMI). This instrument is a 6144×6160 pixels CCD for a

total field of view of 12.5'×12.5', and a pixel scale of 0.12"/pixel (Levine et al. 2012).

At the Las Campanas Observatory in Chile, we used one of the Magellan Twin Telescopes. The Inamori-Magellan Areal Camera & Spectrograph (IMACS) mounted on the Baade telescope is a wide-field imager with eight 2048×4096 pixels CCDs. The short camera mode was selected for a pixel scale of 0.20"/pixel and a 27.4' diameter field.

The lightcurve study was performed at DCT using the VR-filter or r'-filter. The color study was performed with the g'r'i Sloan filters at the Magellan-Baade telescope, and DCT. Our basic observing log is reported in Table 1. The calibration and reduction of our images were performed following the procedure described in Thirouin et al. (2014, 2016). The search for periodicities has been done with the same techniques mentioned in Thirouin et al. (2017). Finally, the color and solar phase curve studies were performed as in Thirouin et al. (2012). For the color study, the best fit aperture radius varied between 4 and 5 pixels for the Magellan-Baade data and was about 3 pixels for the DCT data.

## 3. Photometric results

### 3.1. Color and solar phase curve

Santos-Sanz et al. (2009) observed 2002 CC<sub>249</sub> for color studies with the Very Large Telescope<sup>2</sup> on March 25, 2004 (UT) at a phase angle  $\alpha=0.4^\circ$ . They calculated:  $V-R=0.51\pm0.08$  mag,  $R-I=0.69\pm0.06$  mag,  $V-I=1.20\pm0.07$  mag, and found a spectral gradient of  $22.3\pm8.5\%/100$  nm. They also derived the absolute magnitudes in the R and V bands using the Bowell formalism and the linear formalism (Santos-Sanz et al. 2009):  $H_V(linear)=6.50\pm0.06$  mag, and  $H_R(linear) = 5.99\pm0.05$  mag, and found a R-magnitude of  $21.87\pm0.05$  mag. It is important to point out that Santos-Sanz et al. (2009) did not know the lightcurve of 2002 CC<sub>249</sub>, and thus they have not removed the brightness variation due to rotation for their color estimates. Their data have been

<sup>1</sup>Orbital elements from the Minor Planet Center, August 2017.

<sup>2</sup>Santos-Sanz et al. (2009) used the Antu unit at the Very Large Telescope (ESO-VLT, Cerro Paranal, Chile). They used the FORS1 detector and Bessel broadband BVRI filters. Details can be found in Santos-Sanz et al. (2009)

obtained over about 20 min. With such a short duration<sup>3</sup>, they were not able to notice the large amplitude, and slow rotation of 2002 CC<sub>249</sub>.

Most of our data have been obtained with a VR-broadband filter, and thus are not ideal for color study nor solar phase curve study. However, we have two sets of color data<sup>4</sup> suitable for these studies. Unfortunately, the g' and i' bands observed at DCT have an insufficient quality to be included here, only the r' band will be used for the solar phase curve of 2002 CC<sub>249</sub>. The phase function is:

$$\phi(\alpha) = 10^{-0.4\alpha\beta} \quad (1)$$

with  $\alpha$  as phase angle and  $\beta$  as the phase coefficient at  $\alpha < 2^\circ$ . Based our Magellan and DCT data, the range of phase angles is limited with observations of 2002 CC<sub>249</sub> at  $0.6^\circ$  and  $1^\circ$  for color study. However, by including Santos-Sanz et al. (2009) data, the solar phase curve of 2002 CC<sub>249</sub> is over a phase angle range between  $0.4^\circ$  and  $1^\circ$ . Based on Smith et al. (2002); Sheppard (2012), once can converted the Johnson-Morgan-Cousins colors (BVRI, used by Santos-Sanz et al. (2009)) to the Sloan colors (g'r'i'z'):  $V-R=0.59(g'-r')+0.11$ , and  $R-I=1.00(r'-i')+0.21$ . Using previous equations, Santos-Sanz et al. (2009) obtained  $g'-r'=0.68$  mag, and  $r'-i'=0.48$  mag.

The absolute magnitude ( $H_{r'}$ ) is the object's magnitude assuming that the object is at 1 AU from the Sun ( $r_h$ ) and the Earth ( $\Delta$ ) and at  $\alpha=0^\circ$ :

$$H_{r'} = m_{r'}(1, 1, \alpha = 0^\circ) = m_{r'} - 5 \log(r_h \Delta) - \alpha\beta \quad (2)$$

where the corrected r'-band magnitude is  $m_{r'}(1, 1, \alpha)$ . With brightness variations due to rotation, and the distance removed, we obtain:  $\beta = 0.54 \pm 0.05$  mag/ $^\circ$ ,  $H_{r'} = 6.15 \pm 0.05$  mag (Figure 1). However, the value from Santos-Sanz et al. (2009) is not corrected from brightness variation as the rotational phase for this point cannot be estimated securely. In fact, even if we are able to predict the rotational phase of the Santos-Sanz et al. (2009) data, the propagation of the uncertainty for the rotational

period estimate is to be considered. On the other hand, because these two datasets are separated by more than 13 years, we may also have to consider that the lightcurve have changed over the years due to change in the system geometry (or pole orientation if it is a single object). Therefore, there is an uncertainty of  $\pm 0.4$  mag for Santos-Sanz et al. (2009) data due to the brightness variation of the object (error bar due to brightness not plotted in Figure 1 for clarity). In conclusion, our phase curve is not optimal and more data are required to provide a clear and secure solar phase curve.

We also use our Magellan dataset for color study and report:  $g'-i'=1.24 \pm 0.05$  mag,  $g'-r'=0.97 \pm 0.06$  mag, and  $r'-i'=0.27 \pm 0.06$  mag. In conclusion, 2002 CC<sub>249</sub> displays an ultra red surface characteristic of a dynamically cold classical TNO based on the Santos-Sanz et al. (2009) study and this work.

### 3.2. Lightcurve

Our dataset is composed of three isolated nights in 2016 as well as two isolated and three consecutive nights in 2017. During our observations in 2016, only fragments of the lightcurve of 2002 CC<sub>249</sub> were obtained. Our longest run was  $\sim 3.7$  h, and only one maximum of the curve with an amplitude of about 0.5 mag was observed. Therefore, a long rotational period ( $P > 8$  h, assuming a double-peaked lightcurve) was suspected. One maximum and one minimum were observed on UT March 18, 2017, and two minima and one maxima on UT March 30. Both nights allowed us to constrain the rotational period to approximately 12 h assuming a double-peaked lightcurve.

We applied a light-time correction to our observing runs. The highest peak of the Lomb periodogram is at 4.04 cycles/day (5.94 h), and the PDM method confirms such a peak (Figure 1). The next step is to select the best option between single- and double-peaked lightcurve (i.e. period of 5.94 h or 11.87 h).

Generally, the albedo contributions is up to 20% for asteroids and TNOs (Degewij et al. 1979; Sheppard et al. 2008; Thirouin et al. 2010). Some TNOs like Eris, Makemake, or Haumea have high geometric albedos between 51% and 96% (Sicardy et al. 2011; Ortiz et al. 2012, 2017). The lightcurves of Eris and Makemake are mostly

<sup>3</sup>No Julian Date are available in Santos-Sanz et al. (2009), but the data are available in the European Southern Observatory (ESO) archive system at: <http://archive.eso.org/cms.html>.

<sup>4</sup>Data obtained on March 10, 2017 are not considered for the color/phase curve study as the weather conditions were not photometric.

flat because dominated by the nearly spherical shape and/or pole-on orientation of these objects, whereas in the case of Haumea, the lightcurve is dominated by Haumea’s elongated shape, and the dark red spot contribution is only about 10% (Thirouin 2013; Lacerda et al. 2008). Assuming that 2002 CC<sub>249</sub> has a single-peaked lightcurve, albedo variation(s) of about 80% would be required on the object’s surface. This scenario is unlikely, and therefore the single-peaked option seems inadequate. Secondly, by plotting the double-peaked lightcurve, one can appreciate that there is a  $\sim 0.1$  mag asymmetry between the first and second maxima. In conclusion, the double-peaked option is the more adequate for 2002 CC<sub>249</sub>. The double-peaked lightcurve assuming a periodicity of 11.87 h and a full amplitude of  $0.79 \pm 0.04$  mag is plotted over two cycles in Figure 1. In Table 2, we report the photometry used in this work. The zero phase of the lightcurve is the date of the object’s first image (Table 2).

With such a large lightcurve amplitude, 2002 CC<sub>249</sub> can be a contact binary system with a non-equator-on configuration assuming two objects with similar sizes or a single very elongated object close to an equator-on configuration (see Section 4 for more details). A lightcurve with a U-/V-shape at the maximum/minimum of brightness is characteristic of a contact/close binary system with a near equator-on orientation (Sheppard & Jewitt 2004; Lacerda 2011). For 2002 CC<sub>249</sub>, one can note the V-shape at the minima and the second maximum with a U-shape. But, the first maximum displays a sharper peak, and thus the U-shape is not obvious. However, it is important to point out that the first maximum is based on fragmentary datasets obtained in 2016. In Section 4.1, we will discuss the “definition” of the U- and V-shapes.

## 4. Analysis

### 4.1. V-shape and U-shape: definition

Hektor, the largest Jupiter Trojan asteroid, was found to have large amplitude short-term light variations with a characteristic U/V shaped lightcurve (Cook 1971). This U/V shaped rotational lightcurve results from shadowing and viewing geometry effects from a contact binary viewed nearly equator-on (Hartmann & Cruik-

shank 1978; Wijesinghe & Tedesco 1979; Weidenschilling 1980). The U/V shape of a rotational lightcurve for a contact binary asteroid based on viewing geometry and phase angle effects has been further modeled in detail by several authors (Cellino et al. 1989; Lacerda & Jewitt 2007; Gnat & Sari 2010; Descamps 2015). The U-shape for the maximum and V-shape for the minimum peak of a lightcurve is apparent for contact binary asteroids viewed near equator on and at low phase angles, for which the latter occurs for all TNOs.

We here present a simple way to determine if a rotational lightcurve is likely caused by a contact binary object based on the differences in the full-width-at-half-maximum (FWMH) for the maximum (U-shape) and minimum (V-shape) peaks of brightness for the lightcurve. This analysis allows a more quantitative approach than simple visual inspection of a lightcurve without requiring a detailed model of the lightcurve. This analysis is based on the fact that the U-shape maxima of the lightcurve should show a higher FWHM than the V-shape minimum of the lightcurve, if there are differences in the peaks and it is caused by a contact binary. The full peak-to-peak amplitude has been used to estimate the U- and V-FWHM.

We show the FWHM of TNOs with large amplitude lightcurves ( $\Delta m > 0.15$  mag) from Thirouin et al. (2010, 2012, 2014, 2016); Sheppard (2007); Jewitt & Sheppard (2002) and likely contact binaries from Thirouin et al. (2017); Lacerda et al. (2014); Sheppard & Jewitt (2004) in Figure 2. In this Figure, we plot all four FWHM of these objects: two for the U-FWHM for the maximum and two for the V-FWHM for the minimum. It is clear the non-contact binaries or single objects have all of their peaks FWHM less than about 0.30 and near each other whereas the likely contact binaries have U-FWHM greater than about 0.30 and V-FWHM less than about 0.20. The differences between the two types of peaks is usually greater than about 0.1 for their FWHM for the contact binaries, whereas for the non-contact binaries the differences between the various peaks is less than about 0.05.

It appears the maximum and minimum peaks of single objects have similar FWHM peaks throughout the lightcurve, whereas the likely contact binaries have significantly different FWHM for their maximum and minimum peaks. In Figure 2, we

also report the evolution of the V- and U-FWHM of Hektor with the aspect angle of the system (based on Lacerda & Jewitt (2007)). One can appreciate that at high aspect angle, the differences between the two types of peaks is above 0.1, whereas at an aspect angle of  $53^\circ$ , the difference is near 0.1. For lower aspect angles, the difference is less pronounced.

Again, this is just a simple way to quickly assess if an object's lightcurve displays a contact binary nature. A full model of the objects likely shape and configuration is needed to fully analyze an objects lightcurve. In conclusion, we consider that the U/V shape at the maximum/minimum of brightness are significantly different for likely contact binary objects and can be quantitatively looked at by the difference in their FWHM. We find that 2002 CC<sub>249</sub> has over a 0.1 difference in its U-FWHM versus its V-FWHM, signifying it is likely a contact binary like 2001 QG<sub>298</sub>, 2004 TT<sub>357</sub> and possibly 2003 SQ<sub>317</sub> (Figure 2).

#### 4.2. Roche system

The large variability of 2002 CC<sub>249</sub> and its U-/V-shaped lightcurve is best explained if this object is a contact binary.

Following Leone et al. (1984), the mass ratio and the density of the system are estimated (Figure 3). Two extreme options (min and max) are obtained: i) a mass ratio  $q_{min}=0.6$  and density  $\rho_{max}=1 \text{ g cm}^{-3}$  or ii) a mass ratio of  $q_{max}=1$  and density  $\rho_{max}=5 \text{ g cm}^{-3}$ . The uncertainty for the mass ratio is  $\pm 0.05$ . For the rest of the study, conservative mass ratios of  $q_{min}=0.6$ , and  $q_{max}=1$  will be used (reasons presented in Thirouin et al. (2017)).

If 2002 CC<sub>249</sub> is a Roche system with  $q=0.6$ , and  $\rho=1 \text{ g cm}^{-3}$ , the primary's axis ratios are:  $b/a=0.85$ ,  $c/a=0.78$  ( $a=125/55 \text{ km}$ ,  $b=106/47 \text{ km}$ , and  $c=97/43 \text{ km}$  considering a geometric albedo of 0.04/0.20, and  $H=6.15 \text{ mag}$ ), the secondary's axis ratios are:  $b_{sat}/a_{sat}=0.73$ ,  $c_{sat}/a_{sat}=0.67$  ( $a=117/52 \text{ km}$ ,  $b=85/38 \text{ km}$ , and  $c=78/35 \text{ km}$  with an albedo of 0.04/0.20). The value <sup>5</sup> D is 0.81. Therefore, the separation between the components is 299/132 km considering an albedo of 0.04/0.20.

<sup>5</sup> $D=(a+a_{sat})/d$  with the orbital separation (d), and a,  $a_{sat}$  the primary and secondary longest axes respectively

With  $q=1$  and  $\rho=5 \text{ g cm}^{-3}$ , the axis ratios of the primary are:  $b/a=0.97$ ,  $c/a=0.95$ , and the secondary's ones are:  $b_{sat}/a_{sat}=0.97$ ,  $c_{sat}/a_{sat}=0.95$ , and  $D=0.41$ .

A density of  $5 \text{ g cm}^{-3}$  is improbable for an object with a diameter in the 200-400 km range, and especially for an object at the edge of our Solar System. Therefore, the option considering  $\rho=1 \text{ g cm}^{-3}$  is favored. But, only several lightcurves obtained at different system's geometries will be required to model the system and improve our estimates.

#### 4.3. Jacobi ellipsoid

A Fourier series (second order, generally able to reproduce lightcurves due to shape) failed to reproduce the lightcurve, since the lightcurve is not a simple sinusoid but has an U-/V-shape to it (Figure 1). This is why we prefer the contact binary hypothesis.

However, following we also present a study assuming that 2002 CC<sub>249</sub> is a Jacobi ellipsoid.

Following Binzel et al. (1989), the lightcurve amplitude ( $\Delta m$ ) of a Jacobi with  $a>b>c$  and in rotation along the c-axis varies as:

$$\Delta m = 2.5 \log \left( \frac{a}{b} \right) - 1.25 \log \left( \frac{a^2 \cos^2 \xi + c^2 \sin^2 \xi}{b^2 \cos^2 \xi + c^2 \sin^2 \xi} \right) \quad (3)$$

Considering an aspect angle ( $\xi$ ) of  $90^\circ$ , we estimate the object's elongation,  $a/b=2.07$ , and  $c/a=0.37$  ( $c/a$  ratio estimated based on Chandrasekhar (1987)). Therefore, using the previous axis ratio estimates and the absolute magnitude reported in this work, we compute:  $a=373/167 \text{ km}$ ,  $b=180/81 \text{ km}$ , and  $c=138/62 \text{ km}$  using 0.04/0.20 as albedo values and  $\xi=90^\circ$ .

With  $\xi=60^\circ$ , we derive an elongation larger than 2.31 indicating that the object is unstable to fission due to rotation (Sheppard 2004; Jeans 1919). Therefore, if 2002 CC<sub>249</sub> is a Jacobi ellipsoid, its viewing angle has to be between  $76^\circ$  and  $90^\circ$ .

Assuming an equatorial view and based on Chandrasekhar (1987), we compute the lower density limit:  $\rho \geq 0.34 \text{ g cm}^{-3}$ . Such a low value favors an icy composition. This result is compatible with thermal modeling of TNOs from Herschel Space Observatory and/or Spitzer, suggesting a highly

porous surface for these outer Solar System objects (Lellouch et al. 2013; Vilenius et al. 2014).

## 5. Summary

Based on images carried out using the Lowell’s Discovery Channel Telescope and the Magellan-Baade Telescope in 2016 and 2017, we summarize our results as follows:

- 2002 CC<sub>249</sub> has an asymmetric double-peaked lightcurve with a U-/V-shape at the maximum/minimum of brightness, a periodicity of 11.87 h, and a peak-to-peak amplitude of 0.79 mag. This extreme variability is best interpreted by a contact binary. 2002 CC<sub>249</sub> is the first contact binary candidate in the dynamically Cold Classical population. This is surprising as the largest fraction of wide binaries is in this population.
- Assuming a contact binary, two main solutions are found: i)  $q_{min}=0.6$ , and  $\rho_{min}=1$  g cm<sup>-3</sup> or ii)  $q_{max}=1$ , and  $\rho_{max}=5$  g cm<sup>-3</sup>.
- Because a density of  $\rho=5$  g cm<sup>-3</sup> is doubtful for 2002 CC<sub>249</sub>, we prefer the option with  $q=0.6$ , and  $\rho=1$  g cm<sup>-3</sup>. With this option, we find:  $b/a=0.85$ ,  $c/a=0.78$  for the primary, and  $b_{sat}/a_{sat}=0.73$ ,  $c_{sat}/a_{sat}=0.67$  for the secondary. We calculate that the components are separated by 299/132 km (using 0.04/0.20 as albedo range).
- If 2002 CC<sub>249</sub> is a Jacobi in hydrostatic equilibrium, we estimate:  $\rho\geq 0.34$  g cm<sup>-3</sup>, and  $a/b=2.07$ , assuming a viewing angle  $\xi=90^\circ$ . Its viewing angle must be between  $76^\circ$  and  $90^\circ$ , if 2002 CC<sub>249</sub> is rotationally stable.
- We report a new color study confirming that 2002 CC<sub>249</sub> has an ultra red surface, like most Cold Classical objects.
- Contact binaries (likely/confirmed) present maxima of brightness (U-shape) with a larger full width at half maximum (FWHM), and smaller minima of brightness (V-shape) FWHM than single objects. The FWHM of the contact binaries U-shape is larger than 0.30, whereas other objects have a  $FWHM\leq 0.28$ . The V-shape has a FWHM

generally less than 0.21 for the (likely/confirmed) contact binaries. The FWHM difference in minimum and maximum peaks is greater than about 0.1 for contact binaries, and less than 0.05 for other objects, when the viewing angle is near equator-on. In the case of 2002 CC<sub>249</sub>, the U-FWHM are 0.33 and 0.30 whereas the V-FWHM are 0.19 and 0.20 (one value per peak).

We would like to thank the referee for a careful reading of this paper and very useful comments. This research is based on data obtained at the Lowell Observatory’s Discovery Channel Telescope (DCT). Lowell operates the DCT in partnership with Boston University, Northern Arizona University, the University of Maryland, and the University of Toledo. Partial support of the DCT was provided by Discovery Communications. LMI was built by Lowell Observatory using funds from the National Science Foundation (AST-1005313). We acknowledge the DCT operators: Andrew Hayslip, Heidi Larson, Teznie Pugh, and Jason Sanborn. A special thank to Jason for dealing with some technical difficulties during our DCT runs. This paper includes data gathered with the 6.5 m Magellan-Baade Telescope located at las Campanas Observatory, Chile. Audrey Thirouin is partly supported by Lowell Observatory funding. Authors acknowledge support from the National Science Foundation, grant number AST-1734484 awarded to the “Comprehensive Study of the Most Pristine Objects Known in the Outer Solar System”.

## REFERENCES

- Batygin, K., Brown, M. E., & Fraser, W. C. 2011, *ApJ*, 738, 13
- Benecchi, S. D., Noll, K. S., Grundy, W. M., et al. 2009, *Icarus*, 200, 292
- Binzel, R. P., Farinella, P., Zappala, V., & Cellino, A. 1989, *Asteroids II*, 416
- Brown, M. E. 2001, *AJ*, 121, 2804
- Brown, M. E. 2013, *ApJ*, 778, L34
- Cellino, A., Zappala, V., & Farinella, P. 1989, *Icarus*, 78, 298

- Chandrasekhar, S. 1987, New York : Dover, 1987.
- Cook, A. F. 1971, NASA Special Publication, 267, 155
- Degewij, J., Tedesco, E. F., & Zellner, B. 1979, *Icarus*, 40, 364
- Descamps, P. 2015, *Icarus*, 245, 64
- Gladman, B., Marsden, B. G., & Vanlaerhoven, C. 2008, *The Solar System Beyond Neptune*, 43
- Gnat, O., & Sari, R. 2010, *ApJ*, 719, 1602
- Hartmann, W. K., & Cruikshank, D. P. 1978, *Icarus*, 36, 353
- Jeans, J. H. 1919, Cambridge, University press, 1919.
- Jewitt, D. C., & Sheppard, S. S. 2002, *AJ*, 123, 2110
- Lacerda, P., & Jewitt, D. C. 2007, *AJ*, 133, 1393
- Lacerda, P., Jewitt, D., & Peixinho, N. 2008, *AJ*, 135, 1749
- Lacerda, P. 2011, *AJ*, 142, 90
- Lacerda, P., McNeill, A., & Peixinho, N. 2014, *MNRAS*, 437, 3824
- Lellouch, E., Santos-Sanz, P., Lacerda, P., et al. 2013, *A&A*, 557, A60
- Leone, G., Paolicchi, P., Farinella, P., & Zappala, V. 1984, *A&A*, 140, 265
- Levine, S. E., Bida, T. A., Chylek, T., et al. 2012, *Proc. SPIE*, 8444, 844419
- Levison, H. F., & Stern, S. A. 2001, *AJ*, 121, 1730
- Noll, K. S., Grundy, W. M., Chiang, E. I., Margot, J.-L., & Kern, S. D. 2008a, *The Solar System Beyond Neptune*, 345
- Noll, K. S., Grundy, W. M., Stephens, D. C., Levison, H. F., & Kern, S. D. 2008b, *Icarus*, 194, 758
- Ortiz, J. L., Sicardy, B., Braga-Ribas, F., et al. 2012, *Nature*, 491, 566
- Ortiz, J. L., Santos-Sanz, P., Sicardy, B., et al. 2017, *Nature*, 550, 219
- Peixinho, N., Lacerda, P., & Jewitt, D. 2008, *AJ*, 136, 1837
- Santos-Sanz, P., Ortiz, J. L., Barrera, L., & Boehnhardt, H. 2009, *A&A*, 494, 693
- Sheppard, S. S. 2004, Ph.D. Thesis, University of Hawaii.
- Sheppard, S. S., & Jewitt, D. 2004, *AJ*, 127, 3023
- Sheppard, S. S. 2007, *AJ*, 134, 787
- Sheppard, S. S., Lacerda, P., & Ortiz, J. L. 2008, *The Solar System Beyond Neptune*, 129
- Sheppard, S. S. 2012, *AJ*, 144, 169
- Sicardy, B., Ortiz, J. L., Assafin, M., et al. 2011, *Nature*, 478, 493
- Smith, J. A., Tucker, D. L., Kent, S., et al. 2002, *AJ*, 123, 2121
- Thirouin, A., Ortiz, J. L., Duffard, R., et al. 2010, *A&A*, 522, A93
- Thirouin, A., Ortiz, J. L., Campo-Bagatin, A., et al. 2012, *MNRAS*, 424, 3156
- Thirouin, A. 2013, Ph.D. Thesis, University of Granada.
- Thirouin, A., Noll, K. S., Ortiz, J. L., & Morales, N. 2014, *A&A*, 569, A3
- Thirouin, A., Sheppard, S. S., Noll, K. S., et al. 2016, *AJ*, 151, 148
- Thirouin, A., Sheppard, S. S., Noll, K. S. 2017, *ApJ*, 844, 135.
- Vilenius, E., Kiss, C., Müller, T., et al. 2014, *A&A*, 564, A35
- Weidenschilling, S. J. 1980, *Icarus*, 44, 80
- Wijesinghe, M. P., & Tedesco, E. F. 1979, *Icarus*, 40, 383

Table 1: UT-Dates (MM/DD/YYYY), the number of images (Nb.) obtained each night, the heliocentric ( $r_h$ ), and geocentric ( $\Delta$ ) distances in astronomical units (AU), the phase angle ( $\alpha$ , in degrees) of the observations, the filter(s) used, and the telescope are reported in this Table.

Geocentric, heliocentric distances and phase angle are from the Minor Planet Center Ephemeris generator.

UT-date	Nb.	$r_h$ [AU]	$\Delta$ [AU]	$\alpha$ [°]	Filter	Telescope
02/14/2016	23	38.059	37.334	1.0	VR	DCT
04/06/2016	19	38.056	37.066	0.2	VR	DCT
05/11/2016	1+1+1	38.054	37.312	1.0	g'r'i'	DCT
05/13/2016	16	38.054	37.334	1.1	VR	DCT
03/10/2017	12	38.036	37.106	0.5	r'	DCT
03/18/2017	38	38.036	37.064	0.3	VR	DCT
03/19/2017	3	38.036	37.061	0.3	VR	DCT
03/20/2017	20	38.036	37.056	0.3	VR	DCT
03/30/2017	67	38.035	37.037	0.0	VR	DCT
04/24/2017	2+2+2	38.034	37.116	0.6	g'r'i'	Magellan



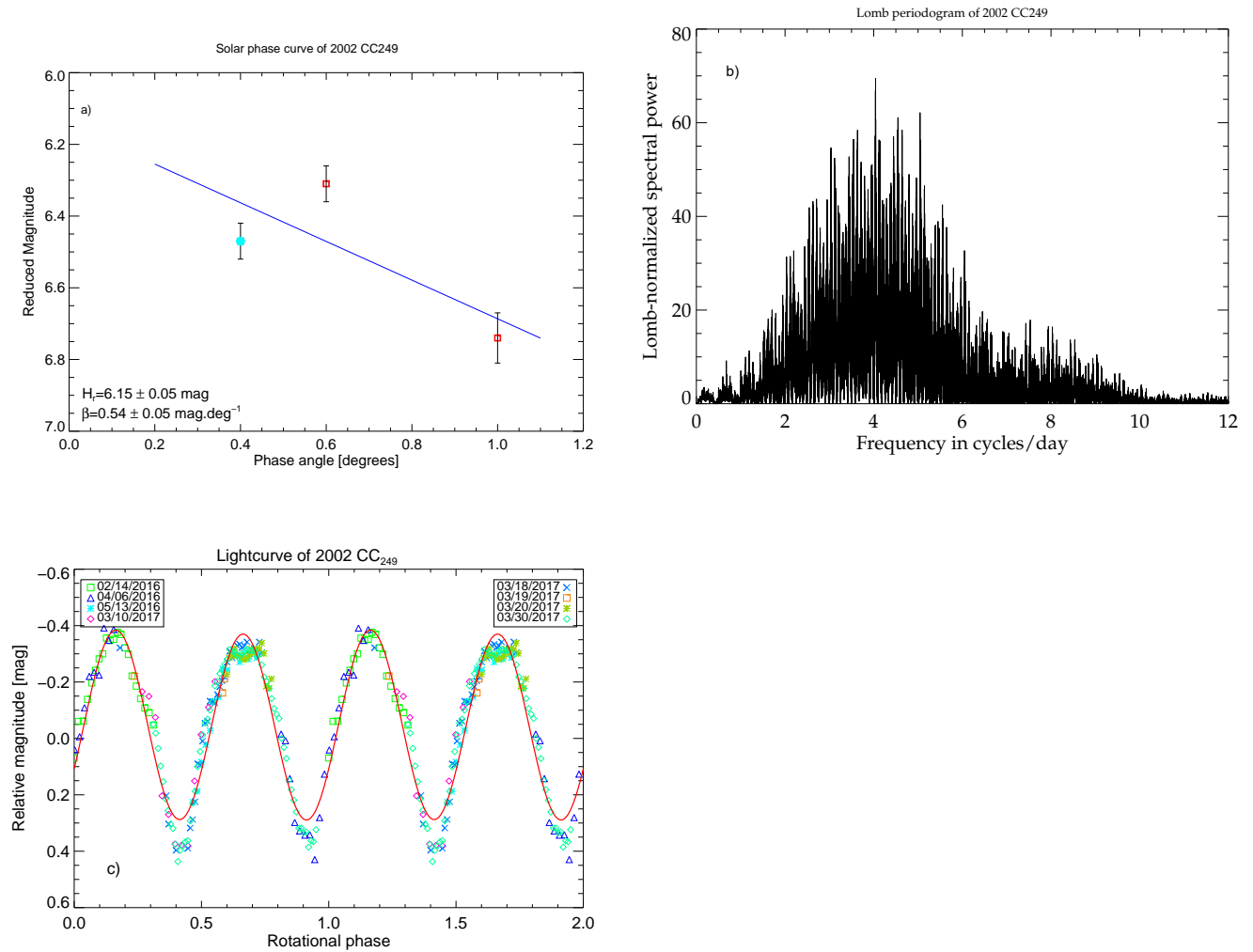


Fig. 1.— *Solar Phase curve, Lomb periodogram, and lightcurve of 2002 CC<sub>249</sub>*: The solar phase curve (a)) is plotted using our data (red square), and Santos-Sanz et al. (2009) result (cyan circle). The peak with the highest spectral power of the Lomb periodogram is located at 4.04 cycles/day (b)). The double-peaked lightcurve is plotted over two rotations. The 2<sup>nd</sup> order Fourier series (red continuous line) is not able to reproduce the V- and U-shape of the curve (c)). Error bars are not plotted for clarity, but the typical error bar is  $\pm 0.05$  for the photometry

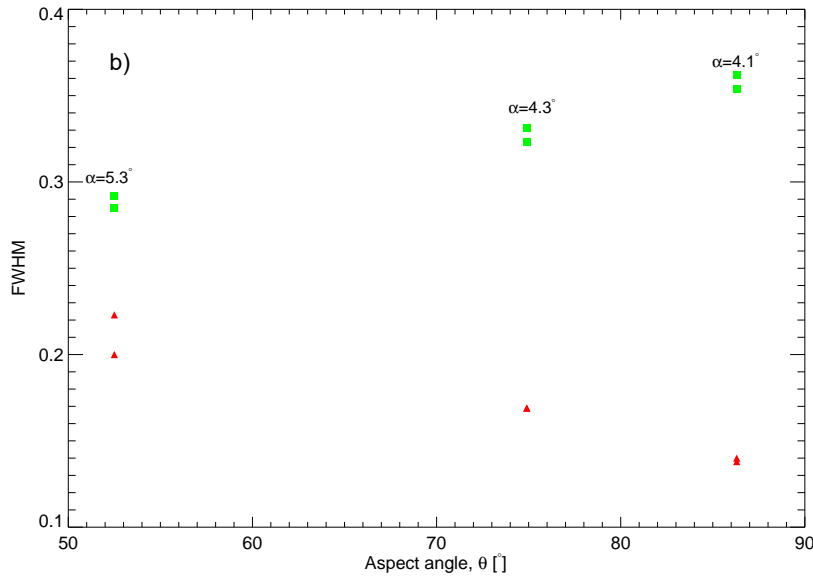
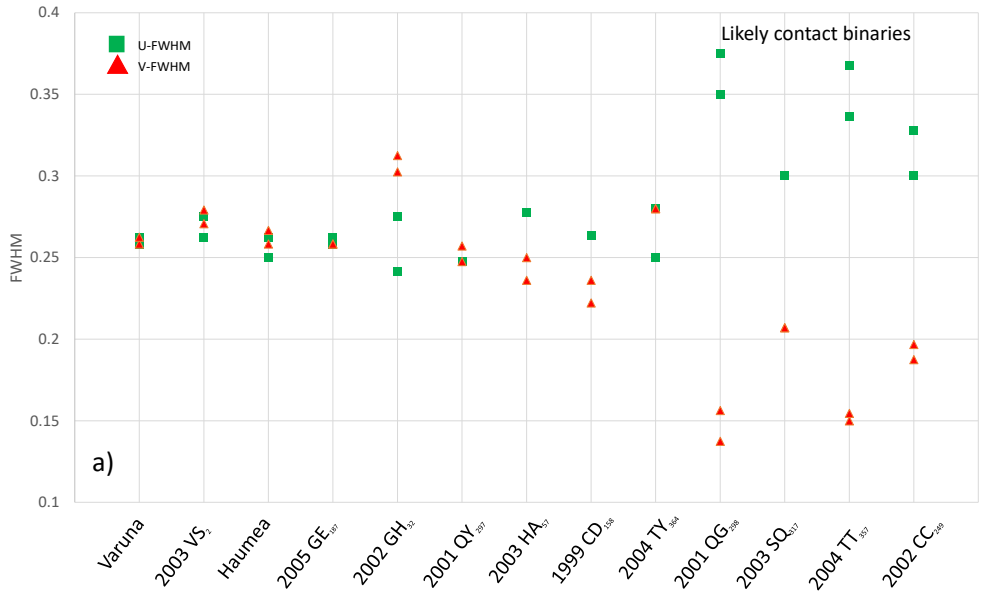


Fig. 2.— Full width at half maximum (FWHM) of single objects, resolved binaries and (likely/confirmed) contact binaries. Plot a): The FWHM of the maxima (U-FWHM) and of the minima (V-FWHM) of several objects are reported. Only double-peaked lightcurve with a amplitude larger than 0.15 mag are considered. We report the FWHM of both peaks (4 points per object), but in some cases both peaks have the same FWHM. The non-contact binary objects have a U-FWHM  $\leq 0.28$  whereas the (likely/confirmed) contact binaries present a U-FWHM  $\geq 0.30$ . The V-FWHM is  $\leq 0.21$  for the (likely/confirmed) contact binaries. The minima and maxima FWHM peak differences are greater than about 0.1 for contact binaries and less than 0.05 for other objects. 2001 QG<sub>298</sub> is the only confirmed contact binary (Sheppard & Jewitt 2004). Plot b): The U-/V-FWHM of the Jupiter Trojan Hektor versus the aspect angle of the system are plotted. Phase angles ( $\alpha$ ) are also indicated for each dataset. One can appreciate that the FWHM differences are greater than 0.1 at large aspect angle, and is about 0.1 for an aspect angle around 53°. Same legend for both plot.

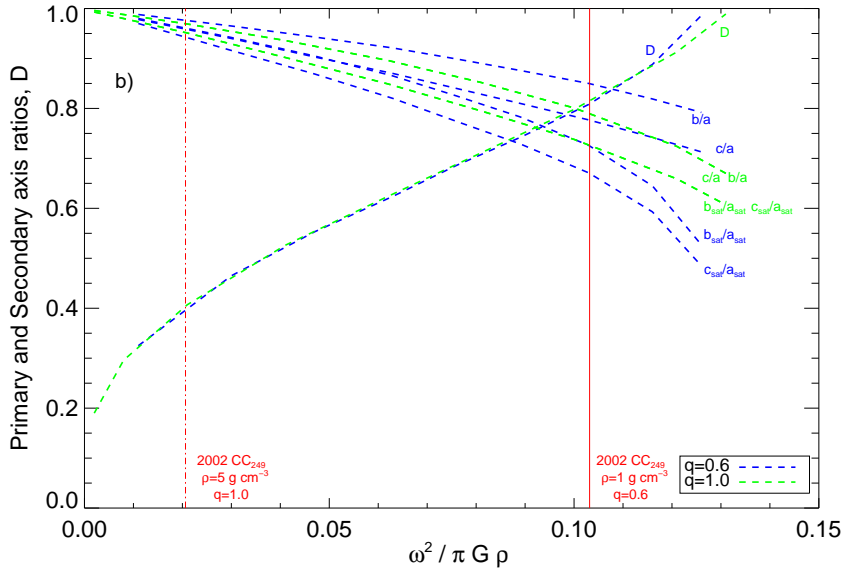
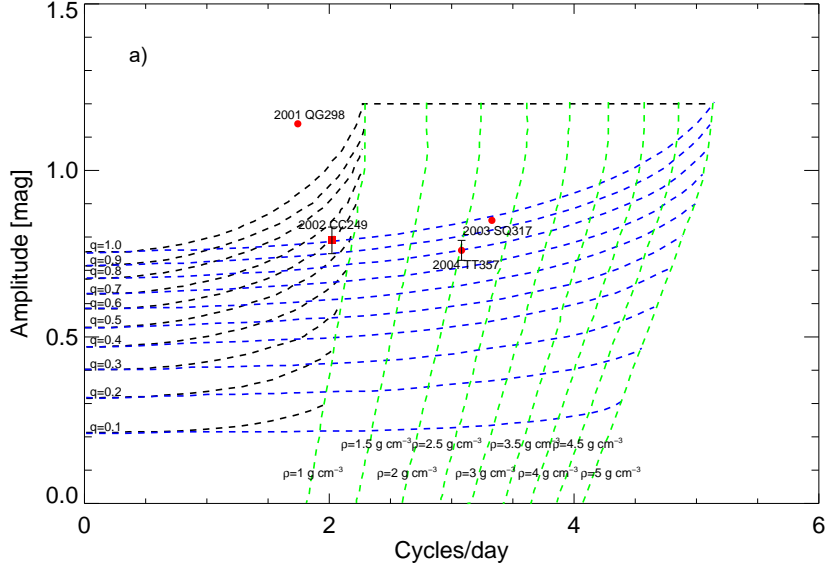


Fig. 3.— The network of Roche sequences (plot a)), adapted from Leone et al. (1984)), and axis ratios of the components, and parameter  $D$  (plot b)): 2002 CC<sub>249</sub> (red square) can have a mass ratio of 1, and a density of  $5 \text{ g cm}^{-3}$ , or a mass ratio of 0.6 and a density of  $1 \text{ g cm}^{-3}$ . Axis ratios of the primary ( $b/a$ ,  $c/a$ ), of the secondary ( $b_{\text{sat}}/a_{\text{sat}}$ ,  $c_{\text{sat}}/a_{\text{sat}}$ ), and parameter  $D$  for a mass ratio of 0.6 (blue), and 1 (green). The red dot-dash line is 2002 CC<sub>249</sub> assuming a mass ratio of 1, and the red continuous line is using a mass ratio of 0.6. See Leone et al. (1984); Thirouin et al. (2017) for more details about the network of Roche sequences.

TABLE 2

PHOTOMETRY USED IN THIS PAPER IS AVAILABLE IN THE FOLLOWING TABLE. JULIAN DATE IS WITHOUT LIGHT-TIME CORRECTION.

Object	Julian Date	Relative magnitude [mag]	Error [mag]
2002 CC <sub>249</sub>	2457432.88848	0.07	0.07
	2457432.89676	-0.06	0.14
	2457432.90608	-0.06	0.04
	2457432.91436	-0.14	0.03
	2457432.92265	-0.20	0.03
	2457432.92979	-0.24	0.03
	2457432.93689	-0.28	0.03
	2457432.94402	-0.30	0.03
	2457432.95111	-0.36	0.03
	2457432.95824	-0.35	0.03
	2457432.96535	-0.35	0.03
	2457432.97247	-0.38	0.03
	2457432.97957	-0.37	0.04
	2457432.98669	-0.32	0.04
	2457432.99382	-0.30	0.05
	2457433.00095	-0.22	0.04
	2457433.00922	-0.19	0.04
	2457433.01751	-0.14	0.04
	2457433.02579	-0.11	0.04
	2457433.03407	-0.09	0.05
	2457433.04235	-0.05	0.05
	2457484.73942	-0.02	0.11
	2457484.74778	0.01	0.16
	2457484.75619	0.14	0.16
	2457484.76586	0.30	0.13
	2457484.77536	0.33	0.13
	2457484.78552	0.34	0.10
	2457484.79505	0.34	0.10
	2457484.80463	0.43	0.12
	2457484.81407	0.28	0.17
	2457484.82355	0.13	0.19
	2457484.83300	0.04	0.13
	2457484.84244	-0.01	0.08
	2457484.85189	-0.11	0.05
	2457484.86134	-0.22	0.05
	2457484.87078	-0.23	0.07
	2457484.88023	-0.22	0.06
	2457484.88968	-0.39	0.05

TABLE 2—*Continued*

Object	Julian Date	Relative magnitude [mag]	Error [mag]
	2457484.89912	-0.35	0.08
	2457484.90858	-0.39	0.09
	2457521.67318	0.23	0.04
	2457521.68144	0.19	0.04
	2457521.68972	0.08	0.04
	2457521.69799	0.02	0.03
	2457521.70626	-0.03	0.03
	2457521.71453	-0.13	0.03
	2457521.72279	-0.15	0.03
	2457521.73104	-0.25	0.03
	2457521.73931	-0.24	0.03
	2457521.74772	-0.30	0.03
	2457521.75598	-0.29	0.03
	2457521.76425	-0.27	0.03
	2457521.77250	-0.30	0.03
	2457521.78076	-0.28	0.03
	2457521.78911	-0.31	0.03
	2457521.79737	-0.29	0.03
	2457822.85438	-0.17	0.06
	2457822.86735	-0.15	0.07
	2457822.88009	-0.07	0.06
	2457822.89282	0.20	0.09
	2457822.90551	0.27	0.09
	2457822.91818	0.37	0.09
	2457822.93084	0.38	0.11
	2457822.94353	0.38	0.13
	2457822.95619	0.15	0.10
	2457822.96892	-0.01	0.11
	2457822.98330	-0.11	0.12
	2457822.99580	-0.20	0.08
	2457830.81664	0.20	0.05
	2457830.82097	0.30	0.05
	2457830.83066	0.40	0.05
	2457830.83544	0.39	0.05
	2457830.84025	0.32	0.06
	2457830.84503	0.29	0.05
	2457830.85821	0.22	0.05
	2457830.86299	0.09	0.05
	2457830.86780	0.09	0.05

TABLE 2—*Continued*

Object	Julian Date	Relative magnitude [mag]	Error [mag]
	2457830.87258	0.01	0.04
	2457830.87740	-0.05	0.04
	2457830.88218	-0.06	0.04
	2457830.88699	-0.13	0.05
	2457830.89178	-0.13	0.04
	2457830.89659	-0.13	0.04
	2457830.89659	-0.16	0.04
	2457830.90138	-0.18	0.04
	2457830.90619	-0.20	0.04
	2457830.91097	-0.22	0.04
	2457830.91579	-0.27	0.04
	2457830.92057	-0.31	0.04
	2457830.92538	-0.29	0.04
	2457830.93017	-0.30	0.05
	2457830.93498	-0.33	0.07
	2457830.93977	-0.33	0.07
	2457830.94457	-0.32	0.04
	2457830.94939	-0.33	0.03
	2457830.95420	-0.34	0.04
	2457830.95900	-0.30	0.05
	2457830.96380	-0.31	0.06
	2457830.96861	-0.32	0.07
	2457830.97339	-0.31	0.07
	2457830.97821	-0.34	0.08
	2457830.98299	-0.30	0.08
	2457831.71589	-0.22	0.03
	2457831.74388	-0.16	0.04
	2457831.91506	-0.21	0.04
	2457832.90838	-0.23	0.03
	2457832.91319	-0.28	0.04
	2457832.91797	-0.29	0.05
	2457832.92279	-0.32	0.06
	2457832.92758	-0.30	0.07
	2457832.93238	-0.29	0.07
	2457832.93718	-0.29	0.08
	2457832.94198	-0.28	0.08
	2457832.94677	-0.28	0.03
	2457832.95159	-0.29	0.04
	2457832.95637	-0.32	0.05

TABLE 2—*Continued*

Object	Julian Date	Relative magnitude [mag]	Error [mag]
	2457832.96118	-0.30	0.06
	2457832.96596	-0.32	0.07
	2457832.97078	-0.32	0.07
	2457832.97557	-0.34	0.08
	2457832.98037	-0.30	0.08
	2457832.98516	-0.18	0.03
	2457832.98997	-0.18	0.04
	2457832.99476	-0.21	0.04
	2457842.66412	-0.05	0.04
	2457842.66890	-0.02	0.03
	2457842.67372	0.04	0.03
	2457842.67851	0.10	0.04
	2457842.68331	0.15	0.04
	2457842.68810	0.21	0.04
	2457842.69288	0.26	0.04
	2457842.69767	0.30	0.04
	2457842.70247	0.32	0.04
	2457842.70727	0.38	0.04
	2457842.71206	0.44	0.04
	2457842.71684	0.40	0.04
	2457842.72163	0.38	0.04
	2457842.72642	0.37	0.03
	2457842.73123	0.36	0.04
	2457842.73602	0.29	0.03
	2457842.74080	0.23	0.03
	2457842.74559	0.19	0.03
	2457842.75038	0.10	0.03
	2457842.75519	0.05	0.03
	2457842.75998	-0.01	0.02
	2457842.76476	-0.05	0.02
	2457842.76955	-0.07	0.02
	2457842.77433	-0.10	0.02
	2457842.77914	-0.13	0.02
	2457842.78394	-0.19	0.02
	2457842.78872	-0.20	0.02
	2457842.79351	-0.23	0.02
	2457842.79829	-0.24	0.02
	2457842.80310	-0.26	0.02
	2457842.80789	-0.28	0.02

TABLE 2—*Continued*

Object	Julian Date	Relative magnitude [mag]	Error [mag]
	2457842.81267	-0.32	0.02
	2457842.81747	-0.31	0.02
	2457842.82225	-0.31	0.02
	2457842.82706	-0.30	0.02
	2457842.83185	-0.29	0.02
	2457842.83663	-0.30	0.02
	2457842.84142	-0.31	0.02
	2457842.84620	-0.32	0.02
	2457842.85102	-0.31	0.02
	2457842.85581	-0.31	0.02
	2457842.86059	-0.31	0.02
	2457842.86538	-0.29	0.02
	2457842.87016	-0.30	0.02
	2457842.87498	-0.26	0.02
	2457842.87977	-0.22	0.02
	2457842.88455	-0.20	0.02
	2457842.88934	-0.18	0.02
	2457842.89412	-0.14	0.02
	2457842.89894	-0.11	0.02
	2457842.90373	-0.09	0.02
	2457842.90851	-0.07	0.02
	2457842.91330	0.00	0.02
	2457842.91808	0.03	0.03
	2457842.92289	0.07	0.03
	2457842.92767	0.15	0.03
	2457842.93247	0.18	0.03
	2457842.93726	0.22	0.03
	2457842.94204	0.26	0.04
	2457842.94685	0.32	0.04
	2457842.95163	0.32	0.03
	2457842.95642	0.33	0.04
	2457842.96122	0.33	0.04
	2457842.96600	0.39	0.04
	2457842.97081	0.36	0.05
	2457842.97559	0.37	0.05
	2457842.98041	0.32	0.05



